 © 2007 ASCE

PRESSURE-INDUCED SUBSURFACE SEDIMENT TRANSPORT IN THE SURF ZONE

Ole Secher Madsen and William McKinney Durham

Ralph M. Parsons Laboratory, Department of Civil & Environmental Engineering
Massachusetts Institute of Technology, Cambridge, MA 02139-4307
osm@mit.edu and durham@mit.edu

Abstract: The horizontal pressure gradient associated with the steep front of forward-leaning breaking waves is transmitted into the porous bottom to depths far exceeding the depth of the shear-stress-induced surficial transport sheet flow layer. The horizontal pressure gradient induces a flow within the bed which exerts a seepage force on the soil-skeleton. If sufficiently large the seepage force will cause a failure of the soil matrix and displace subsurface sediment grains, i.e. result in a subsurface sediment transport. This paper investigates the pressure-induced subsurface transport mechanism experimentally by photographically recording the displacement profile of subsurface lightweight sediment grains during passage of the steep front of breaking waves. A simple theoretical model for the dynamic response of subsurface sediments in failure is developed and provides predicted displacement profiles in reasonable agreement with measurements. The potential importance of the subsurface sediment transport mechanism is discussed.

INTRODUCTION

The pressure distribution on the bottom underneath forward-leaning near-breaking or broken waves is transmitted into the porous bed, where it induces a flow. This pressure-induced porous media flow extends to depths into the bed scaled by the horizontal scale of the pressure distribution and exerts a seepage force on the sediment grains within the bed. The horizontal component of this seepage force is related to the horizontal pressure gradient of the pressure distribution on the bottom and is therefore particularly pronounced under the steep front of a forward-leaning breaking wave and may, if sufficiently large, cause a soil-mechanics-type failure of the bed. This mechanism of a pressure-induced subsurface failure during passage of breaking waves was first

Copyright ASCE 2007

Downloaded 15 Feb 2010 to 18.84.5.4. Redistribution subject to ASCE license or copyright; see http://www.ascelibrary.org

identified by Madsen (1974) who, based on a simple model akin to models used for the prediction of slope stability in geotechnical engineering, hypothesized that this failure mechanism could explain the burial of tracer particles to considerable depths below the sediment-fluid interface in the surf zone. He argued, however, that this failure mechanism would have an insignificant effect on sediment transport rates in the surf zone because it would merely reduce the critical shear stress for initiation of motion from τ_{cr} to 0 with τ_{cr} reasonably expected to be far smaller than the bottom shear stress, τ_b, under breaking waves, i.e. $\tau_b - \tau_{cr} \approx \tau_b$, and hence an insignificant effect on surficial shear-stress-induced sheet flow transport.

Drake and Calantoni (2001) developed a sophisticated granular flow model for the bottom-shear-stress-induced surficial sediment transport, referred to as sheet flow transport, under forward-leaning breaking waves. They found that inclusion of a forcing term related to the pressure gradient under the steep front of a breaking wave had a pronounced effect on the surficial sediment transport rates predicted by their model. Following their lead, Hoefel and Elgar (2003) subsequently succeeded in predicting on-shore bar migration by including a pressure gradient transport term in their empirical sediment transport formulation.

The renewed interest in pressure-gradient-associated sediment transport processes in the surf zone and the delicate balance between on- and off-shore transport rates for equilibrium beach profile predictions, prompted us to revisit the subsurface pressure-induced failure mechanism and its potential contribution to sediment transport rates in the surf zone. This time, however, a more extensive experimental investigation is carried out, as described in the first section of this paper. Also, the simple soil mechanics subsurface failure analysis, presented by Madsen (1974), is extended to include the dynamic response of the subsurface sediment in failure. This model is described in the subsequent section and affords an approximate prediction of the displacement of subsurface sediment grains caused by the passage of the steep front of a forward-leaning breaking wave. Finally, we show that the simple approximate model is capable of predicting experimentally observed displacements reasonably well; and we conclude with a discussion of the potential importance of the subsurface pressure-gradient-induced sediment transport rate relative to the shear-stress-induced surficial sheet flow transport rate in the surf zone. The reader interested in more details of this study than the page-limitation allows us to present here, is referred to Durham (2007).

EXPERIMENTAL INVESTIGATION

Experiments were conducted in the 30m-long, 0.9m-deep and 0.76m-wide wave flume in the J. Robert Gunther Environmental Fluid Mechanics Laboratory in the Ralph M. Parsons Laboratory. The wave flume is equipped with a programmable piston-type wave maker and has a 1 on 10 sloping absorber beach. An instrument carriage runs along the length of the flume on rails that are mounted on top of the frames that support the flume's glass sidewalls.

The Experimental Set-up

The experimental set-up, show in Figure 1, consists of a horizontal shelf made of marine

Copyright ASCE 2007

Downloaded 15 Feb 2010 to 18.84.5.4. Redistribution subject to ASCE license or copyright; see http://www.ascelibrary.org

plywood that forms a "false bottom" 25 cm above the actual flume bottom. Waves climb a 1 on 6 sloping ramp and enter the shelf where breaking is triggered. The breaking wave travels over the first section of the shelf before it enters the test section, which consists of a 10cm-wide, 100cm-long and 15cm-deep Lucite tray installed into the false bottom along the centerline of the flume. To prevent lateral loss of sediment during experiments the tray is covered by gauze, and to allow determination of longitudinal transport, sediment collection bags are installed at each end of the tray.

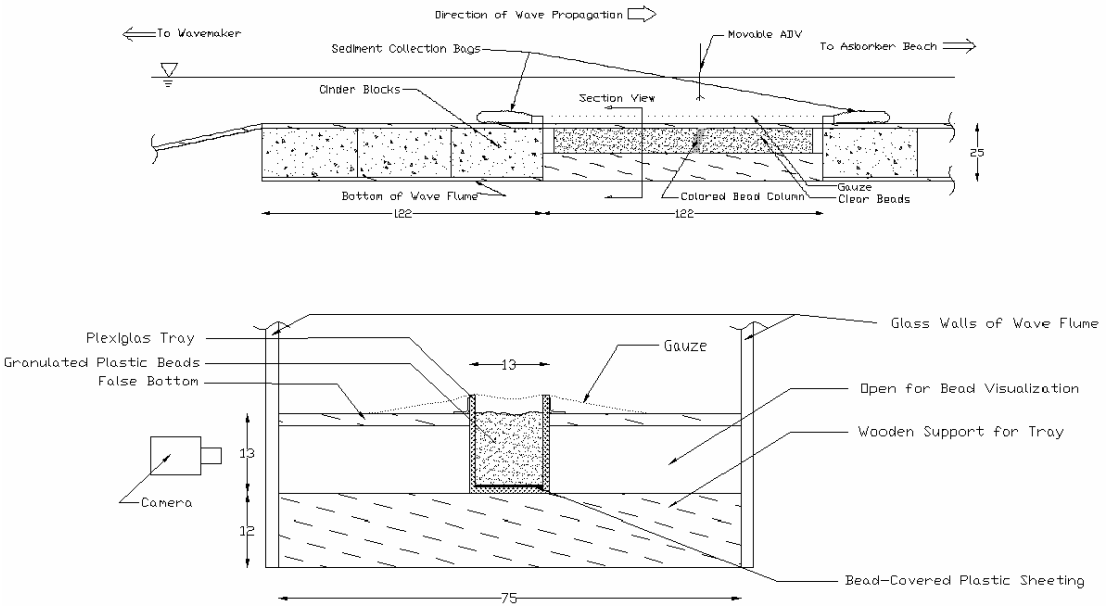

Fig. 1. Experimental Set-up (all dimensions in cm)

The Lucite tray protrudes below the false bottom and contains the sediment, making the sediment bed directly observable through the flume's glass sidewalls. The subsurface movement of a ~2cm-long column of colored sediment inserted in the sediment bed, at the midpoint of the test section, is recorded photographically using a Canon PowerShot S230 digital camera for both stills and video (with a frame rate of 15 frames per second). From the videos, shot during passage of a breaking wave, frame by frame analysis determines when the sediment column starts to move, when it reaches its maximum forward deflection, and when it comes to rest after the wave has passed. Since we are recording the displacement of the column of colored beads along the sidewalls of the Lucite tray, we cut a slice along the centerline of the Lucite tray, by inserting a thin Lucite sheet into the bed, to see if the observed displacements along the sidewall were representative of the displacements over the entire width of the column of colored beads. As evidenced by the still photos shown in Figure 2, we have in this manner verified the validity of our experimental procedure for the determination of subsurface, pressure-gradient-induced movements of a sediment bed.

Since the experimental conditions simulate two-dimensional conditions, the smooth sidewalls of the Lucite tray allow a near-frictionless movement of the sediment grains in contact with the sidewalls, i.e. reproduce two-dimensional conditions. The bottom of the

Copyright ASCE 2007

Downloaded 15 Feb 2010 to 18.84.5.4. Redistribution subject to ASCE license or copyright; see http://www.ascelibrary.org

Lucite tray is covered by sediment grains glued to the surface of a thin plastic sheet. Preliminary experiments showed that the entire sediment bed would slide along the bottom when this was left smooth. With the roughened bottom, the near-bottom sediments in the Lucite tray remained immobile during the experiments (see Figure 2).

The initial "top" of the column of colored sediments coincides with initial sediment fluid interface and is covered from view by the false plywood bottom. However, after passage of several waves a sharp interface between the top of the column of colored sediments, now covered by plain sediment, is clearly visible (Figure 2(b) and (c)). Thus, as conjectured previously in the Abstract, the pressure-gradient-induced subsurface transport, represented by the displacement of the column of colored sediments, extends to much greater depth within the bed than the thickness of the sheer-stress-induced surficial sheet flow, which is responsible for the shaving off of the top portion of the column of colored sediments.

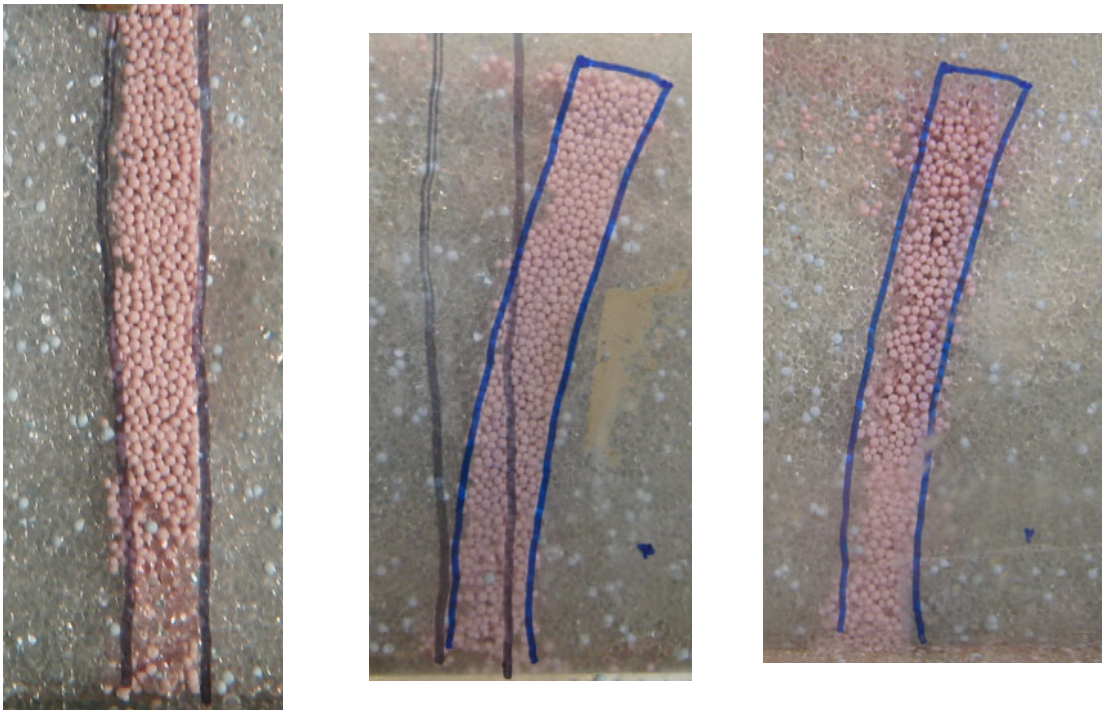

(a) (b) (c)

Fig. 2. Still Photos of the Colored Sediment Column Inserted in the Sediment Bed. (a) Before; (b) After waves (along sidewall); (c) After waves (along centerline)

The Sediment

Madsen (1974) showed that pressure-induced bed failure would occur if the bottom pressure gradient exceeded a critical value given by

Copyright ASCE 2007 Coastal Sediments '07

Downloaded 15 Feb 2010 to 18.84.5.4. Redistribution subject to ASCE license or copyright; see http://www.ascelibrary.org

$$\left|\frac{\partial p}{\partial x}\right|_{crit} = \left(\rho_s(1-n) - \rho(1-n)\right)g\tan\varphi = \left(\rho_b - \rho\right)g\tan\varphi \qquad (1)$$

where ρ_s and ρ are the sediment and fluid densities, respectively, n is the porosity, g is gravity, φ is the internal friction angle of the sediment which is assumed cohesionless, and ρ_b is the density of the saturated bed. To maximize the subsurface pressure-gradient-inducing displacements and make these detectable in our small scale laboratory experiments, a light-weight "sediment", Polyethylene Terephthalate (PET), was chosen. The relevant physical characteristics of this sediment were determined to be: diameter = d = 1.1 ± 0.1 mm, density = ρ_s = 1.27 ± 0.01 g/cm^3, porosity = n = 0.37 ± 0.02, so ρ_b = 1.17 ± 0.01 g/cm^3 and angle of internal friction φ = 34°.8 ± 1° and 39°.2 ± 1°.1 for loosely and densely packed deposits, respectively. The characteristics of the colored PET beads were determined to be essentially identical to those listed above, and a surfactant (Windex) was added to the water to prevent the beads from sticking together.

The Waves

To maximize our ability to stop the experiment after any number of waves, the experiments were performed programming the wave maker to generate solitary waves. The near-bottom orbital velocity as the breaking waves pass over the test section was measured with a Sontek ADV system sampling at a rate of 25Hz. Assuming the breaking waves to be of near-permanent form, i.e. taking $\partial/\partial t \cong -c\partial/\partial x$ with c denoting the phase velocity of the wave, the smoothed time-series of near-bottom horizontal velocity, $u(t)$, provides an estimate of the associated bottom pressure gradient, since we have

$$-\frac{\partial p}{\partial x} = \rho\left(\frac{\partial u}{\partial t} + u\frac{\partial u}{\partial x}\right) \cong \rho\frac{\partial u}{\partial t}\left(1 - \frac{u}{c}\right) \qquad (2)$$

Furthermore, by replacing $-\partial p/\partial x$ by $c^{-1}\partial p/\partial t$, (2) may be integrated to obtain the temporal bottom pressure variation $p(t)$ from which the spatial variation of the bottom pressure, $p(x)$, is obtained by replacing t by $-x/c$. Figure 3 shows the smoothed record of the measured near-bottom horizontal velocity $u(t)$ and the corresponding temporal variation of bottom pressure and pressure gradient obtained from (2) by ensemble averaging 10 wave realizations. For the phase velocity we took c = 1.5 m/s, the average of the measured speed of the crest (1.6 m/s) and the predicted phase velocity for our solitary wave (1.4 m/s). It is noted that the maximum experimental pressure gradient shown in Figure 3, ~180 dynes/cm, exceeds the critical pressure gradients predicted from (1), 116 dynes/cm and 136 dynes/cm for φ = 34.°8 and 39.°2, respectively. Thus, bed failure should occur and, as evidenced by the photos in Figure 2, it obviously did.

Copyright ASCE 2007

Downloaded 15 Feb 2010 to 18.84.5.4. Redistribution subject to ASCE license or copyright; see http://www.ascelibrary.org

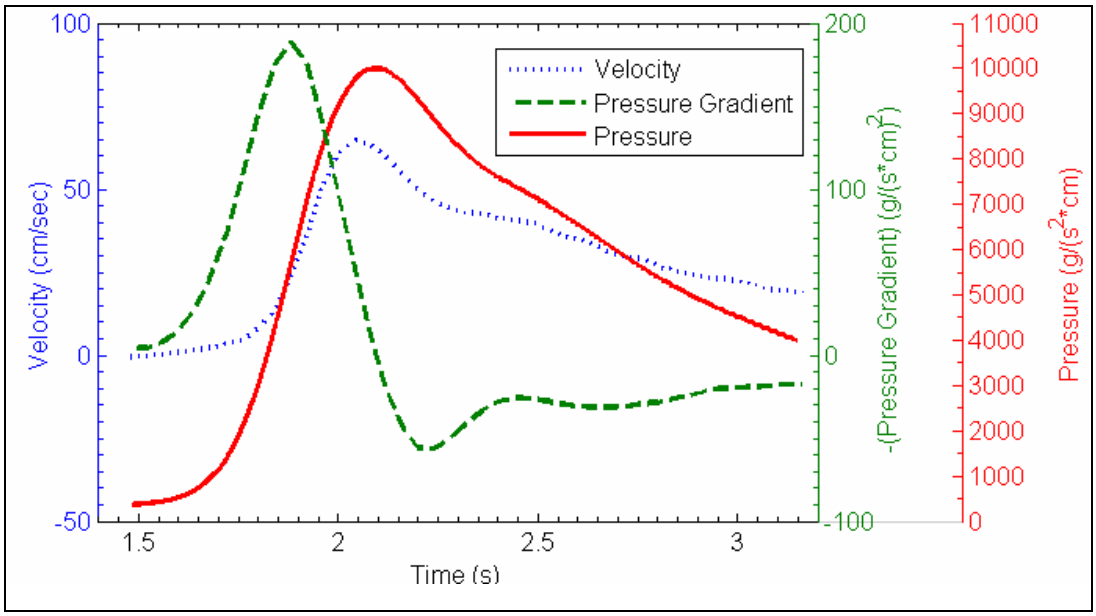

Fig. 3. Experimental Wave Characteristics.

THEORETICAL MODEL

The theoretical model is based on the principles adopted by Madsen (1974), i.e. pressure-induced subsurface failure is assumed to take place along circular arcs, slip circles, as shown in Figure 4.

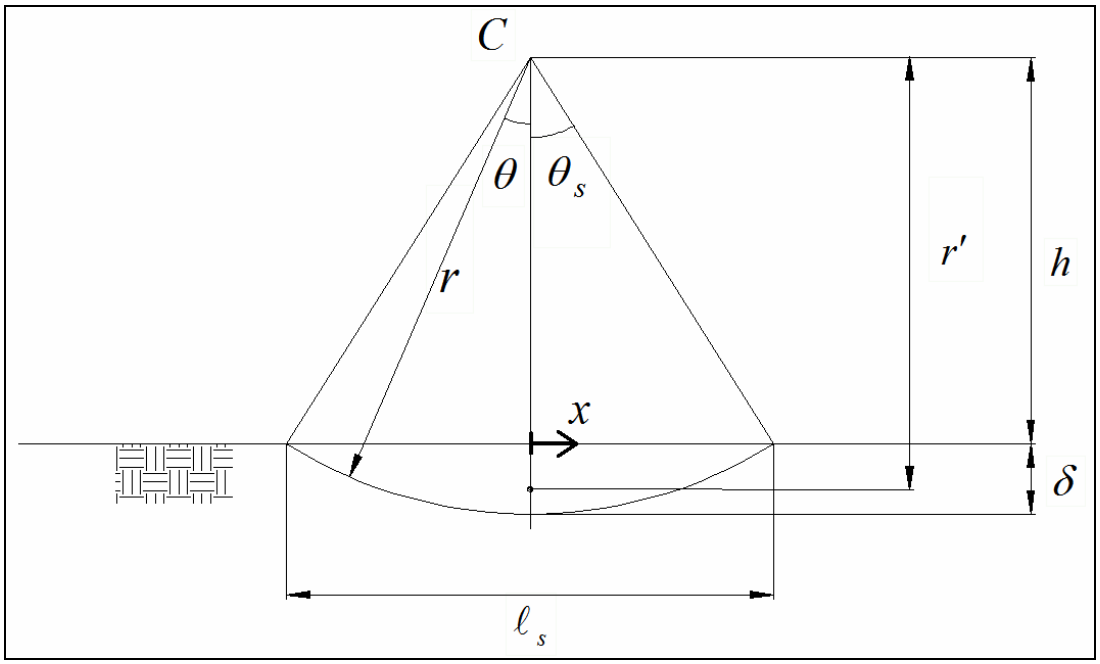

Fig. 4. Slip Circle Characteristics

From Madsen's (1974) analysis of effective stresses along the slip circle, it follows that

Copyright ASCE 2007

Downloaded 15 Feb 2010 to 18.84.5.4. Redistribution subject to ASCE license or copyright; see http://www.ascelibrary.org

the maximum moment around the slip circle's center, C, due to shear stresses corresponding to failure along the slip circle (the "stabilizing" moment) is approximately

$$M_s = 2(\rho_b - \rho) g r^3 \sin\theta_s (1 - \theta_s \cot\theta_s) \tan\varphi \tag{3}$$

where the slip circle's radius = $r = h + \delta$, h being the distance of C above the bottom and δ the maximum depth of the slip circle below the bottom, and the angle

$$\theta_s = Arc\cos\left(\frac{h}{r}\right) \tag{4}$$

The length of the bottom segment within the slip circle is

$$l_s = \frac{2\delta \sin\theta_s}{1 - \cos\theta_s} \tag{5}$$

and it is over this distance, l_s, that the wave-associated bottom pressure acts and produces a moment around C as the bottom pressure distribution $p(x)$ translates past l_s at speed c. This moment, the "driving" moment, is a function of time and is given by

$$M_d(t) = \int_{-l_s/2}^{l_s/2} p(x) x dx = \int_{t+l_s/2c}^{t-l_s/2c} p(t')(ct')cdt' \tag{6}$$

with $p(t)$ as show in Figure 3.

Madsen (1974) determined the characteristics of the limiting slip circle by equating the maximum driving moment obtained from (6) for a specified value of $l_s = l_{smax}$ to the stabilizing moment given by (3), Madsen (1974, Eq. (15)). Here we obtain $l_{smax} = c\Delta t$ where Δt, the time interval during which the pressure gradient exceeds its critical value given by (1), is obtained from Figure 3. With this value of $l_s = l_{smax}$ balancing M_{dmax} and M_s produces the limiting slip circle along which the sediment just reaches failure at the instant when $M_d(t) = M_{dmaz}$. With all slip circles being concentric, for kinematic reasons, any slip circle contained within the limiting slip circle will experience failure for some short period during passage of the pressure distribution associated with the breaking wave.

Figure 5 shows the temporal variation of M_d, the driving moment, and the corresponding value of the maximum realizable stabilizing moment, M_s, for slip circles identified by their depth of penetration into the bed, δ, relative to that of the limiting slip circle, δ_{smax}.

Copyright ASCE 2007

Downloaded 15 Feb 2010 to 18.84.5.4. Redistribution subject to ASCE license or copyright; see http://www.ascelibrary.org

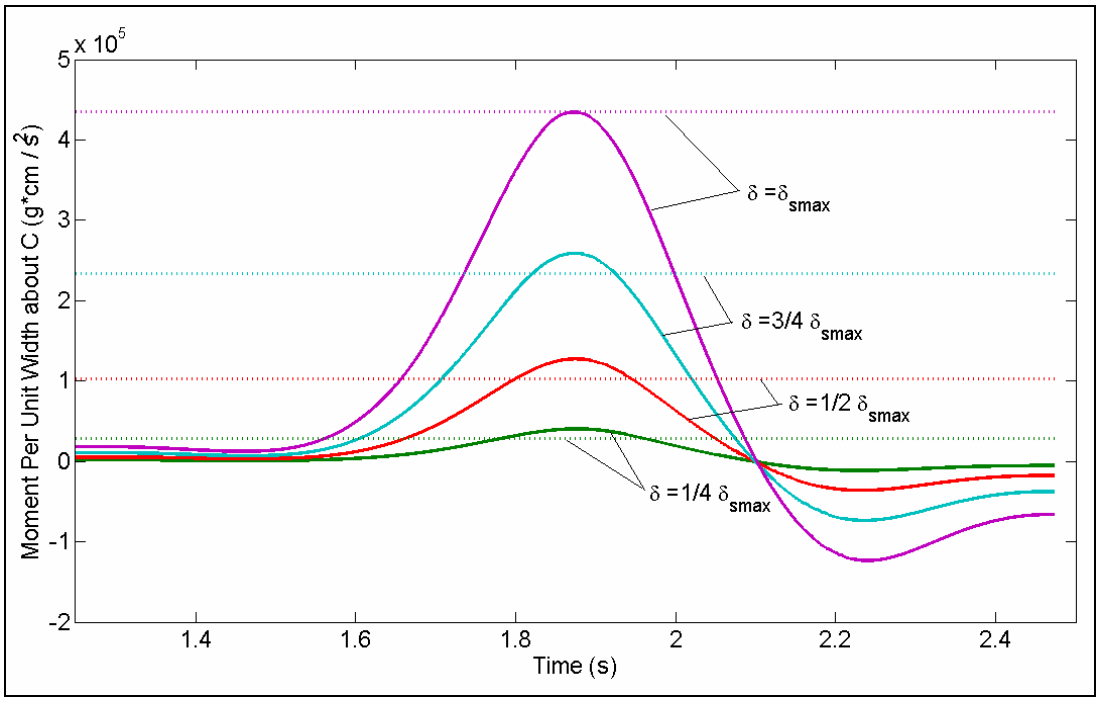

Fig. 5. Temporal Variation of Driving Moments (full lines) and Corresponding Stabilizing Moments (dotted lines) for Different Slip Circles

For the time interval during which $M_d > M_s$ for a particular slip circle, no static moment balance is possible and the bed material above the slip circle responds by rotating around C. As a simple approximate model for the dynamic response of the bed material above a slip circle when $M_d > M_s$ we take

$$I\frac{d^2\theta}{dt^2} + mgr'\theta = M_d(t) - M_s \tag{7}$$

where I is the radial moment of inertia of the bed material above the slip circle of radius r around C

$$I = \frac{r^4}{4}\left(2\theta_s - \sin 2\theta_s + \frac{2}{3}\sin 2\theta_s \sin^2\theta_s\right)\rho_b \tag{8}$$

The mass of the bed material above the slip circle is

$$m = \frac{r^2}{2}(2\theta_s - \sin 2\theta_s)\rho_b \tag{9}$$

and the distance from its center of gravity to C is

Copyright ASCE 2007

Downloaded 15 Feb 2010 to 18.84.5.4. Redistribution subject to ASCE license or copyright; see http://www.ascelibrary.org

$$r' = \frac{4}{3}\frac{\sin^3\theta_s}{2\theta_s - \sin 2\theta_s} r \tag{10}$$

Finally, θ is the rotation angle around C of the material above the slip circle.

With $M_d(t)$ and M_s given for a particular slip circle of radius r, (7) may be solved subject to the initial condition of $\theta = d\theta/dt = 0$ at $t = 0$, and the computation proceeds until $d\theta/dt$ changes sign, i.e. $d\theta/dt = 0$ or $\theta = \theta_{max}$, signifying a change in the sense of rotation and hence a sudden change in the sign of M_s, which always must act in the direction opposite the sense of rotation of the material above. Having solved (7) for a particular value of r, the horizontal displacements of the subsurface sediment a distance of $\delta = r - h$ below the bottom is obtained from

$$\xi = r\theta \le \xi_{\max} = r\theta_{\max} \tag{11}$$

The salient features of this simple model are conceptualized by its graphical representation in Figure 6.

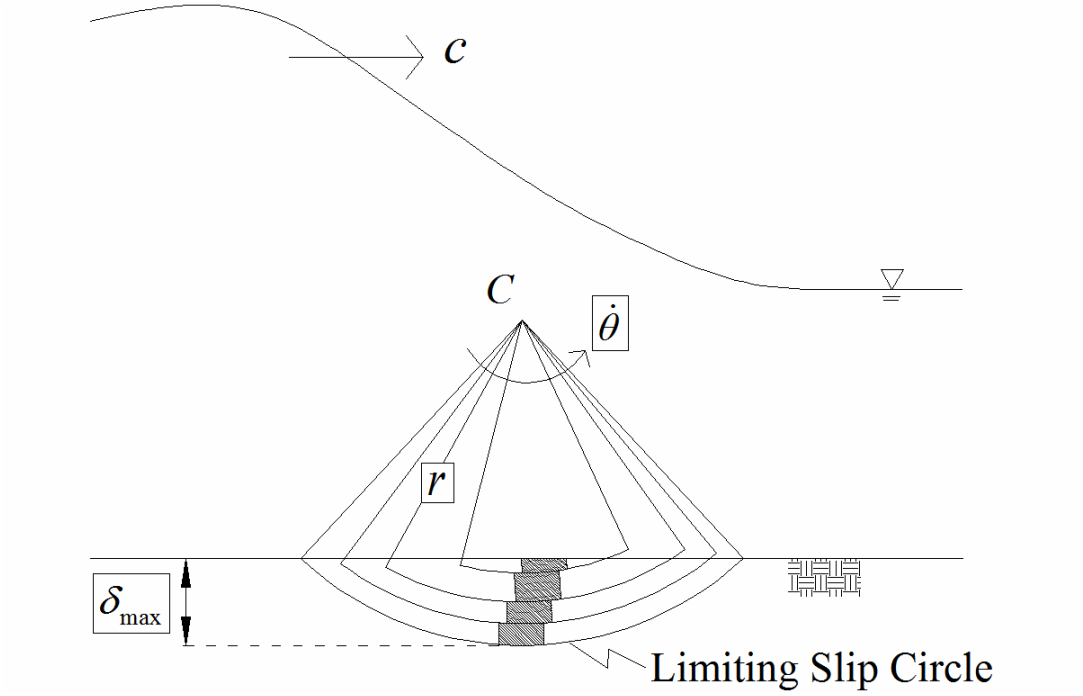

Fig. 6. Conceptual Illustration of the Theoretical Model of Subsurface Sediment Displacements during Failure

RESULTS

From the frame by frame analysis of the videos shot during passage of the steep front face of a forward-leaning breaking wave the displacements of subsurface sediment grains during the period of pronounced bottom pressure gradients are obtained.

Copyright ASCE 2007 Coastal Sediments '07

Downloaded 15 Feb 2010 to 18.84.5.4. Redistribution subject to ASCE license or copyright; see http://www.ascelibrary.org

Ensemble averaged subsurface displacement profiles (from four realizations) are plotted in Figure 7 as a function of number of waves that have passed over an initial "deposited" bed. A striking reduction in the magnitude of the displacement with number of waves is noticed. We conjecture that this reduction is associated with a strengthening of the bed as this is being reworked by the preceding waves, e.g. causing initially weak spots within the soil matrix to become stronger by rearranging individual grains into more stable configurations.

Also shown in Figure 7 are the predicted displacement profiles afforded by our simple theoretical model for the pressure-induced subsurface failure mechanism. The predicted results are shown for various friction angles, φ, which is the only "free parameter" in our model. It is clearly demonstrated that our model predicts a dramatic decrease in displacement as φ, i.e. the strength of the bed material, increases. This lends credence to our conjecture that the observed dramatic decrease in displacements with number of waves is associated with the accumulated reworking and strengthening of the bed material caused by previous waves.

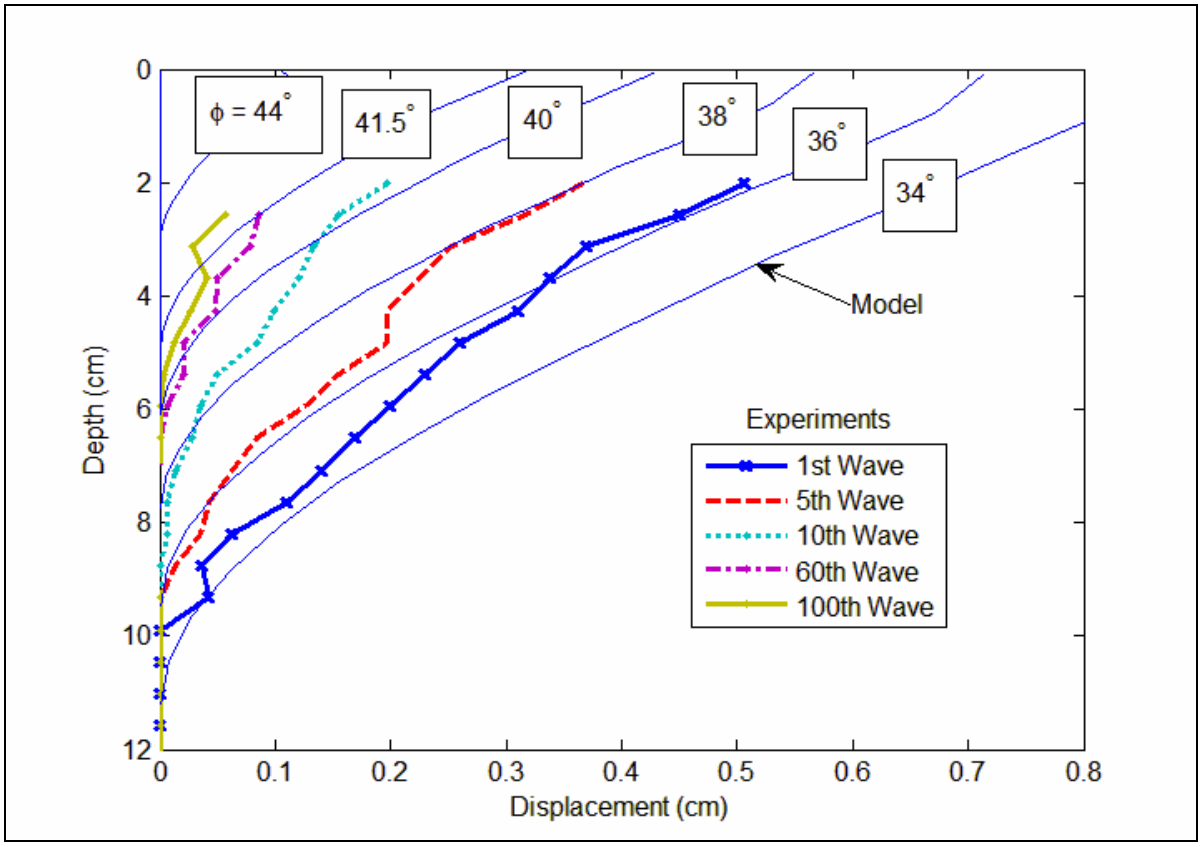

Fig. 7. Subsurface Displacement Profiles Caused by the Passage of the Steep Front Face of a Breaking Solitary Wave

It is particularly encouraging that the predicted displacement profiles are in reasonable agreement with observations for values of the friction angle φ corresponding to those obtained for our sediment, i.e. $\varphi = 34.°8 \pm 1°$ for loosely packed sediments corresponding

Copyright ASCE 2007

Downloaded 15 Feb 2010 to 18.84.5.4. Redistribution subject to ASCE license or copyright; see http://www.ascelibrary.org

to passage of the first wave and φ = 39.°2 ±1.°1 for densely packed sediments corresponding to heavily reworked bed conditions.

A Reality Check

Before getting carried away by the apparent success of our simple model's ability to predict the observed subsurface displacement profiles in Figure 7, it must be emphasized that the observed displacement profiles shown in Figure 7 correspond to the forward subsurface displacements associated with the steep front, i.e. the large pressure gradient peak seen in Figure 3, of the breaking solitary wave passing overhead. Once this pressure gradient "pulse" has passed, the pressure gradient changes sign and drops to values well below the critical value of ~120 dynes/cm^2 predicted by (1). Thus, our simple model would predict that there should be no subsurface failure and hence no backward displacement after the crest of the breaking wave has passed.

But the experiments do not corroborate this prediction! In fact, following the strong forward displacement observed during passage of the steep wave front, the column of colored sediment rebounds, i.e. moves backwards, despite the negligible magnitude of the pressure gradient and comes to rest at a position suggesting the permanent displacement caused by the passage of the entire solitary wave to be but a mere fraction (of the order of one fifth) of the displacement experienced during the passage of the steep front, i.e. the observed displacement shown in Figure 7.

A clue to why this rebound takes place may be found in Figure 2(b) which shows the column of colored beads after the passage of several (~50) solitary waves. Clearly the column, while displaced, is still intact, i.e. individual beads have not been sliding across each other but stayed in contact with their neighbors throughout the experiment. Thus, an actual failure, in the soil mechanics sense, of the subsurface sediments really has not taken place during passage of a breaking wave overhead. If we stipulate that a relative displacement of $\Delta\xi > d$ between adjacent horizontal "layers" of thickness ~d signifies bed failure, since this would allow adjacent sediment grains to change neighbor, we may express a "failure" condition as $\left|\partial\xi/\partial z\right| > 1$, where z is the vertical coordinate. From the displacement profiles shown in Figure 7 we see that $\partial\xi_{\max}/\partial z \leq\sim 0.1$ which supports our conclusion of "no real failure" reached from inspection of the still photos is Figure 2. This need to an angular displacement to exceed a critical value in order for actual failure to take place, appears related to the critical shear condition for irreversibility and the appearance of chaos mentioned by Gollub and Pine (2006).

Thus, the strong pressure gradient under the steep front of the wave has forced the column to deflect in the forward direction but not sufficiently to cause an actual failure. After passage of the wave front the column is left in an unstable state and rebounds in a nearly elastic manner once the force that caused its original deflection is removed. The integrity of the column of colored beads, as it appears along the sidewall of the Lucite tray in Figure 2(b), is somewhat broken up in the middle of the Lucite tray (Figure 2(c)). However, the mixing of beads in the center of the tray may well have been caused by the insertion of the Lucite sheets into the bed during preparation of the center cut.

Copyright ASCE 2007

Downloaded 15 Feb 2010 to 18.84.5.4. Redistribution subject to ASCE license or copyright; see http://www.ascelibrary.org

CONCLUSIONS

Experiments that demonstrate conclusively the existence of a subsurface sediment transport mode under breaking waves were conducted. A simple theoretical model based on soil mechanics principles for failure along slip circles was developed and was capable of predicting, with some success, the observed subsurface displacements caused by the passage of the pressure gradient "pulse" associated with the steep front of a forward-leaning breaking wave. However, the theoretical model did not predict the observed rebound of the subsurface sediments after passage of the crest of the breaking wave. This flaw is believed to be associated with the fact that an actual failure, in the soil mechanics sense, did not take place within the subsurface sediments. Nevertheless, we are confident that the observed (and predicted) subsurface displacements are pressure-gradient-induced. Since a large pressure gradient in the fluid corresponds to large fluid accelerations, this subsurface sediment transport mechanism is indirectly evidence of one of potentially many effects of fluid accelerations in sediment transport processes in the surf zone.

This leaves the all-important question of the importance of this subsurface sediment transport mode relative to the conventional surficial sheet flow transport mode to be answered. To shed some light on this issue, the total sediment transport rate in our experiments was measured by using the ADV system as a bottom profiler. After passage of two solitary waves over an initially plane bed the bottom elevation change (divided by 2 to obtain the value corresponding to passage of a single wave) was measured at 1 cm intervals along three transects for the entire 100cm-length of the Lucite flume. Denoting the measured bottom elevation change associated with passage of a single solitary wave by $\zeta(x)$, the sediment continuity equation

$$q_T(x) = q_{T0} - (1-n)\int_0^x \zeta(x)dx \tag{12}$$

can be used to obtain the total sediment volume transport q_T [cm^3 of sediment per cm width of the tray per solitary wave] by using the amount of sediment captured by the upwave collection bag to determine q_{T0}, the transport at $x = 0$.

The results from ensemble averaging three such experiments for $q_T(x)$ are shown in Figure 8 including the standard deviations of $q_T(x)$. As one would expect $q_{T0} \approx 0$, since the orbital velocity of a solitary wave is purely positive, and q_T increases from $x = 0$ until it reaches a near-constant value of $q_T \approx 3.0$ cm^3/cm for $x > \approx 40$ cm, which is approximately the value of the excursion, $\int_0^\infty u(t)dt$, for our wave. It is noticed that the predicted transport at the end of the tray is in (remarkably) good agreement with the transport inferred from the sediment volume captured in the down-wave collection bag at $x = 100$ cm (indicated by a tick-mark in Figure 8). Thus, we have confidence in our estimate of the total, i.e. surficial as well as subsurface, sediment volume transport per

Copyright ASCE 2007

Downloaded 15 Feb 2010 to 18.84.5.4. Redistribution subject to ASCE license or copyright; see http://www.ascelibrary.org

solitary wave being 3.0 cm^3/cm.

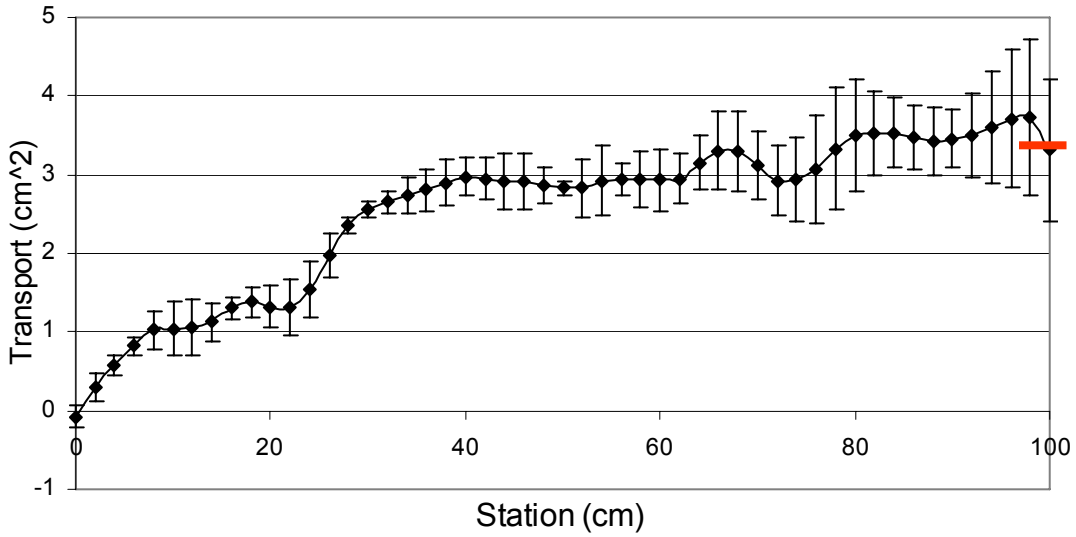

Fig. 8. Measured Total Sediment Volume Transport per Solitary Wave along the Test Section

For comparison, the subsurface sediment transport rate, inferred from the forward displacements during passage of the steep front of the breaking solitary wave (Figure 7), amounts to ~1.3 cm^3/cm for the first and ~0.1 cm^3/cm for the 100^{th} wave. Given the fact that the net subsurface transport rate, i.e. accounting for the "rebound", is lower than the values obtained from Figure 7, by a factor of ~5, it would appear that the subsurface transport rate is at most ~10% of the total. However, this estimate of the relative importance of surficial and subsurface transport rates is obtained for a solitary wave. For a periodic wave the forward velocity (and surficial transport) is followed by a backward velocity (and surficial transport), i.e. a net transport that is a potentially small difference between the forward and backward transport. In contrast, the subsurface transport is exclusively associated with the passage of the steep front of the breaking wave and this should not be significantly different for periodic and solitary waves. We therefore need further experiments involving periodic waves and including the effect of bottom slope, as well as investigations of the behavior of denser sediments (natural sands) during repeated wave-loading, in order to make a final conclusion regarding the potential significance of the contribution of the subsurface sediment transport mechanisms to the total net cross-shore sediment transport rate in the surf zone.

ACKNOWLEDGEMENTS

The support of the Office of Navel Research, Coastal Geosciences Program under Grant Number: N00014-6-1-0318 is gratefully acknowledged as is the assistance of Ms. Lizzie Lundgren who, as a UROP student, conducted some of the experiments and tirelessly analyzed videos, frame by frame, to obtain displacement profiles.

REFERENCES

Drake, T.G. and Calantoni, J. (2001), "Discrete particle model for sheet flow sediment

Copyright ASCE 2007

Downloaded 15 Feb 2010 to 18.84.5.4. Redistribution subject to ASCE license or copyright; see http://www.ascelibrary.org

transport in the nearshore". *J. Geophys. Res., 106*, 19,859-19,868.

Durham, W. M. (2007), "The effect of fluid acceleration on sediment transport in the surf zone", SM Thesis, Department of Civil and Environmental Engineering, MIT, Cambridge, MA 02139., 184p.

Gollub, J. and Pine, D. (2006), "Microscopic irreversibility and chaos", in August Issue of *Physics Today*.

Hoefel, F., and Elgar, S. (2003), "Wave-induced sediment transport and sandbar migration", *Science, 299,* 1885-1887.

Madsen, O.S. (1974), "Stability of a sand bed under breaking waves", in *Proceedings of the 14th International Conference on Coastal Engineering*, ASCE, Reston, Va. 2: 776-794 [also R.M. Parsons Laboratory, Report No. 182, Department of Civil Engineering, MIT, March 1974, 75p.].

Copyright ASCE 2007

Downloaded 15 Feb 2010 to 18.84.5.4. Redistribution subject to ASCE license or copyright; see http://www.ascelibrary.org